International Journal of Heat and Mass Transfer 126 (2018) 1347–1356

Contents lists available at ScienceDirect

International Journal of Heat and Mass Transfer

journal homepage: www.elsevier.com/locate/ijhmt

# $Cu$-$Al_2O_3$/Water hybrid nanofluid through a permeable surface in the presence of nonlinear radiation and variable thermal conductivity via LSM

M. Usman [a], M. Hamid [a], T. Zubair [b], Rizwan Ul Haq [c,*], W. Wang [a]

[a] School of Mathematical Sciences, Peking University, Beijing 100871, PR China
[b] Department of Applied Mathematics and Statistics, Institute of Space Technology, Islamabad 44000, Pakistan
[c] Department of Electrical Engineering, Bahria University, Islamabad Campus, Islamabad 44000, Pakistan

ARTICLE INFO

*Article history:*
Received 30 March 2018
Received in revised form 22 May 2018
Accepted 2 June 2018

*Keywords:*
$Cu$-$Al_2O_3$-water hybrid
Stretching surface
Nonlinear thermal radiation
Variable thermal conductivity
Least square method

ABSTRACT

This paper scrutinizes the significant effects of nonlinear thermal radiation and time-dependent thermal conductivity due to rotating flow of $Cu$-$Al_2O_3$-water hybrid nanofluid over a three-dimension stretching sheet. The influence of bouncy forces and magnetic field are also considered. The obtained set of partial differential equations (PDEs) converted to a simplified set of ordinary differential equations (ODEs) by introducing the feasible similarity transformation. Least square method (LSM) is adopted to examine the solution of developed model. The obtained solutions are compared with the well-known numerical technique: Runge-Kutta method of order fourth (RK-4). Significant influence of various physical parameters on the velocities and temperature are explained in detailed through graphical representations. Behavior of skin friction coefficient and local Nusselt number due the variation of numerous parameters also discussed in detail. The velocity profiles $F'(\eta)$ and $G'(\eta)$ for the case of $Cu$-$Al_2O_3$-water are dominant as compare to $Cu$-water and $Al_2O_3$-water while the fluid temperature is dropped for $Cu$-$Al_2O_3$-water case as compare to $Cu$-water and $Al_2O_3$-water. It is noticed that, variation in the Hartmann, porosity and suction/injection parameters cause to increase the friction at the surface. Opposite behavior of skin friction coefficient is observed by increasing the strength of rotational, Grashof number and slip parameter. Obtained results and comparative study witnesses that the least square technique is well-matched with existing results and it can be applied for complex nature models.



## 1. Introduction

The way to improve the thermal conductivity of any liquid having poor thermal conductivity, is to incorporate the tiny particles (nanoparticles) within the working fluid and this way to improve the thermal conductivity is long lasting and more reliable. Different fluids and various kind of nanoparticles have wide range of applications in different areas of sciences, for instance: exchanger of heat, chemical and biomedical instruments, solar panels and nuclear reactor. When the idea of nanofluid is utilized in cooling schemes of automobiles named as radiator, more than 5% consumption of fuel is improved [1]. Nanofluid contains the tiny particles (nanoparticles) of size less than 100 nm. Many developments are under observation by mean of nanofluid having various classes. A very recent class of nanofluid is "hybrid nanofluid" which is decentralized by incorporating the special class of nanoparticles within the working fluid. Therefore, study of properties, advantages and disadvantages of mixture of two categories of particles is now declared a new task for researchers and scientists. A worthy recent literature related to nanofluids is available [2–8].

The particles of nano type with hybrid technology must be reserved as compared to simple nanoparticles because it required extra care for synthetization process [9–11]. However, this theme is also utilized to formulate different kinds of unique nanoparticles. A very detailed and comprehensive study on this subject is presented by Sarkar et al. [12] and the study of this article explore that properties of hybrid nanofluid. An experimental study which was totally based on suspension of nanoparticles $Al_2O_3$ and micro-encapsulated phase-change are substantial. Ho et al. [13] explained about a very effective relation between density and mass fraction. Furthermore, Botha et al. [14] clarified about the different experiments which was grounded on silver-silica hybrid nanofluid. Numerical study of unsteady and conjugate model in semicircle

* Corresponding author.
*E-mail addresses:* ideal_riz@hotmail.com, r.haq.qau@gmail.com (R. Ul Haq).

https://doi.org/10.1016/j.ijheatmasstransfer.2018.06.005
0017-9310/

**Nomenclature**

| | |
|---|---|
| $u, v, w$ | velocity components |
| $\Omega_0$ | angular velocity of rotating flow |
| $a, b$ | stretching constants |
| $T$ | temperature of the fluid |
| $B_0$ | component of magnetic field |
| $(\rho c_p)_{bf}$ | heat capacity of base fluid |
| $\sigma^*$ | Boltzmann constant |
| $K_p^*$ | porosity |
| $T_\infty$ | ambient fluid temperature |
| $\Omega$ | coefficient of tangential momentum accommodation |
| $\Lambda$ | molecular mean free path |
| $W$ | suction velocity |
| $h_f$ | coefficient of convective heat transfer |
| $\delta$ | slip parameter |
| $k_f$ | thermal conductivity |
| $k^*$ | coefficient of mean absorption |
| $\nu_{hnf}$ | kinematic viscosity of hybrid nanofluid |
| $k_{hnf}$ | variable thermal conductivity of hybrid nanofluid |
| $F, G$ | dimensionless velocity components |
| $\rho_{hnf}$ | density of hybrid nanofluid |
| $\sigma_{hnf}$ | electrical conductivity of hybrid nanofluid |
| $\mu_{hnf}$ | dynamic viscosity of hybrid nanofluid |
| $(\rho c_p)_{hnf}$ | heat capacity of hybrid nanofluid |
| $Ha$ | Hartman number |
| $K_p$ | porosity parameter |
| $\lambda$ | rotating parameter |
| $Gr$ | Grashof number |
| $Pr$ | Prandtl number |
| $T_f$ | temperature of the fluid heating the surface of the surface |
| $Ec$ | Eckert number |
| $Rd$ | radiation parameter |
| $\gamma$ | stretching ratio |
| $S$ | suction ($S > 0$)/injection ($S < 0$), |
| $Bi$ | convective parameters |
| $\beta_{hnf}$ | coefficient of thermal expansion of hybrid nanofluid |
| $\tau_{wx}, \tau_{wy}$ | shear stresses in $x$ and $y$-direction |
| $Nu_x$ | local Nusselt number |
| $\theta(\eta)$ | dimensionless temperature |
| $\theta_w$ | chemical reaction parameter |

cavity with the hybridization of $Al_2O_3$ and Copper ($Cu$) nanoparticles are presented by Chamkha et al. [15]. They have discussed the different aspects of hybrid fluid that contains nanoparticles and announced about the Rayleigh number with high values.

Rotational flow is a very important and significant process because it has wide number of applications in different areas of engineering and science like in rotating category of equipments, flow in anti-cyclonic, centrifugal filtration, food procedures and rotor-stator system dynamics of hurricanes. A well-known expert Crane [16] shaped his research in the field of stretching flow. Later on, Wang [17] provided the impression of rotation of fluid produced by stretching surface. Furthermore, he find out the solution of this problem with the help of perturbation for minor value of parameter $k$. After this, numerous investigators operated on this thoughts and formulated many physical models using different properties of rotating fluid. Takhar et al. [18] modelled the unsteady MHD phenomena of rotating flow over sheet of stretching type. Further, he resolved this problem using numerical method. Andersson [19] deliberated the flow which was slip and passed over stretching surface. He considered Newtonian fluid with linear stretching effects and gave the exact solution of proposed model using analytical technique. Nazar et al. [20] provided the study regarding unsteady rotating phenomena. Eldahab et al. [21] investigated the concepts of rotating fluid flow with suction/blowing on Hydromagnetic heat transfer by mixed convection. Further, recent study can be find through these Refs. [22,23].

The investigation of MHD procedures and their establishment for knowledge on fluid with nanoparticles have now develop very operational and applicable in numerous zones of sciences, engineering and technology. Some of the application are such as treatments of wound, optical modulator, MHD power based generator and etc. Moreover, hypothetical investigation of this field delivers us the information regarding Lorentz force. This category of force is shaped due to the MHD effects which is very helpful theme to regulate the cooling structures. In order to formulate this type of process, Maxwell concepts and Ohm's law are very significant in this regard. The modern concepts regarding this area can be study in [24–29]. Hayat et al. explained the study relevant to this field in [30]. Magnetohydrodynamic study of nanofluid (pseudo-plastic) is presented by Lin et al. [31]. Later, Nadeem et al. [32] studied the squeezing flow with MHD effects for water in which metallic functionalized nanoparticles are considered as base particles.

Radiative fluids belong to special class of fluids that release energy in the form of radiations. This property of fluid is very important in successful completion of many industrial procedures. This class of fluids is applicable in those systems in which ambient fluid and boundary exteriors have vast temperature alterations. Additionally, this study is also valid for many kinds of devices in space science, which can be operate at high temperature level. Commonly, "Stefan-Boltzmann law" of thermal radiation is used to model this type of problems. Micropolar study along with radiation enhancement is studied by Ishak [33]. In the same year, Hayat et al. [34] studied the unsteady phenomena with significant magnetic field effects of radiative fluid. Later on, Shateyi et al. [35] studied the process of geometrical consequences linked with radiative MHD boundary layer and laminar flow. Khan et al. [36] applied his research on radiation heat energy concept with MHD nanofluid properties.

The discussed study in the previous paragraphs is decently devoted with heat transfer of three dimensional MHD rotating flow of $Cu$-$Al_2O_3$/water hybrid nanofluid past a permeable stretching surface with nonlinear thermal radiation and time dependent thermal conductivity. The following key points are disclosed in the motivation of work. The possible solution of the modelled problem is evaluated with least square approach. The accuracy of the suggested technique is proved by a comparative study between LSM solution, numerical scheme (RK-4) and already published. The worthy discussion of outcomes for the behavior of velocity and temperature is presented. It is observed that, the velocity profiles $F'(\eta), G'(\eta)$ for the case of $Cu$-$Al_2O_3$-water are dominant as compare to $Cu$-water and $Al_2O_3$-water while the fluid temperature is dropped for $Cu$-$Al_2O_3$-water case as compare to Cu-water and $Al_2O_3$-water. The influence of physical quantities is also enclosed in our study. It is perceived that, an enhancement in the values of rotation, Grashof and slip parameters shows a drop in the behavior of skin friction coefficient. On the other hand, the variation in the Hartmann, porosity and suction/injection parameters shows an opposite behavior. Graphical study for different parameter and error estimation are also presented to explore the physical circumstances.

## 2. Mathematical and geometrical analysis

Consider the steady, free convection magnetohydrodynamic three-dimensional rotating flow of incompressible nanofluid along a permeable stretching sheet. Further, it is assumed that angular velocity of rotating flow is $\Omega_0$ and magnetic field is applied parallel to $z$-axis. Therefore, the induced magnetic field and electric field are ignored due to small Reynolds number. Effects of Grashof number and nonlinear thermal radiation are considered beside the variable thermal conductivity. In the view of above constraints, the continuity, momentum and energy equations takes the following form [39–40]:

$$\frac{\partial u}{\partial x}+\frac{\partial v}{\partial y}+\frac{\partial w}{\partial z}=0, \tag{1}$$

$$u\frac{\partial u}{\partial x}+v\frac{\partial u}{\partial y}+w\frac{\partial u}{\partial z}-2\Omega_0 v=\nu_{hnf}\frac{\partial^2 u}{\partial z^2}+\frac{g(\rho\beta)_{hnf}}{\rho_{hnf}}(T-T_\infty)-\left(\frac{\sigma_{hnf}B_0^2}{\rho_{hnf}}+\frac{\nu_{hnf}}{K_p^*}\right)u, \tag{2}$$

$$u\frac{\partial v}{\partial x}+v\frac{\partial v}{\partial y}+w\frac{\partial v}{\partial z}+2\Omega_0 u=\nu_{hnf}\frac{\partial^2 v}{\partial z^2}-\frac{g(\rho\beta)_{hnf}}{\rho_{hnf}}(T-T_\infty)-\left(\frac{\sigma_{hnf}B_0^2}{\rho_{hnf}}+\frac{\nu_{hnf}}{K_p^*}\right)v, \tag{3}$$

$$\frac{(\rho c_p)_{hnf}}{(\rho c_p)_{bf}}\left(u\frac{\partial T}{\partial x}+v\frac{\partial T}{\partial y}+w\frac{\partial T}{\partial z}\right)=\frac{1}{(\rho c_p)_{bf}}\frac{\partial}{\partial z}\left(k_{hnf}(T)\frac{\partial T}{\partial z}\right)+\frac{16\sigma^*}{3k^*(\rho c_p)_{bf}}\frac{\partial}{\partial z}\left(T^3\frac{\partial T}{\partial z}\right)+\frac{\mu_{hnf}}{(\rho c_p)_{bf}}\left(\frac{\partial w}{\partial z}\right)^2. \tag{4}$$

The suitable boundary conditions associated with Eqs. (1)–(4) are:

$$\begin{cases} u=ax+\frac{2-\Omega}{\Omega}\Lambda\frac{\partial u}{\partial z}, v=by+\frac{2-\Omega}{\Omega}\Lambda\frac{\partial v}{\partial z}, w=-W, -\frac{\partial T}{\partial z}=\frac{h_{bf}}{k_{bf}}(T_{bf}-T), \\ \text{at } z=0, \\ u, v\to 0, T\to T_\infty, \text{ as } z\to\infty. \end{cases} \tag{5}$$

The thermal boundary conditions for the cold fluid at the upper surface of the plate and at the lower surface of the plate are expressed in Eq. (5) as $-\frac{\partial T}{\partial z}=\frac{h_f}{k_f}(T_f-T)$, which is representing the same behavior of conduction and convection processes. Since, both the fluids are at rest and sheet is stretched to cause the motion of the upper fluid. The hot fluid from the bottom is providing heat to the surface through convective surface. In the direction of $x$, $y$ and $z$ the velocity components are signified by $u$, $v$ and $w$ respectively (see Eqs. (1)–(4)). Also $a$, $b>0$ are stretching constants. Temperature of the fluid, component of magnetic field, heat capacity of base fluid, Boltzman constant, porosity parameter, ambient fluid temperature, coefficient of tangential momentum accommodation, molecular mean free path, suction velocity, coefficient of convective heat transfer, temperature of the fluid heating the surface of the surface, thermal conductivity and coefficient of mean absorption are denoted by $T, B_0^2, (\rho c_p)_{bf}, \sigma^*, K_p^*, T_\infty, \Omega, \Lambda, W>0, h_{bf}, T_{bf}, k_{bf}$ and $k^*$. Furthermore, $\nu_{hnf}, \beta_{hnf}, \rho_{hnf}, \sigma_{hnf}, \mu_{hnf}, (\rho c_p)_{hnf}$ and $k_{hnf}(T)$ are respectively represents the kinematic viscosity, coefficient of thermal expansion, density, electrical conductivity, dynamic viscosity, heat capacity and variable thermal conductivity of hybrid nanofluid which given as [41]:

$$\mu_{hnf}=\frac{\mu_{bf}}{(1-(\phi_1+\phi_2))^{2.5}}, \rho_{hnf}=\phi_1\rho_1+\phi_2\rho_2+(1-\phi)\rho_{bf}, \tag{6}$$

$$(\rho c_p)_{hnf}=\phi_1(\rho c_p)_1+\phi_2(\rho c_p)_2+(1-\phi)(\rho c_p)_{bf}, \tag{7}$$

$$(\rho\beta)_{hnf}=\phi_1(\rho\beta)_1+\phi_2(\rho\beta)_2+(1-\phi)(\rho\beta)_{bf}, \tag{8}$$

$$\frac{k_{hnf}}{k_{bf}}=\frac{\phi_1k_1+\phi_2k_2+2\phi k_{bf}+2\phi(\phi_1k_1+\phi_2k_2)-2\phi^2k_{bf}}{\phi_1k_1+\phi_2k_2+2\phi k_{bf}-\phi(\phi_1k_1+\phi_2k_2)+\phi^2k_{bf}}, \tag{9}$$

$$\frac{\sigma_{hnf}}{\sigma_{bf}}=1+\frac{3\phi(\phi_1\sigma_1+\phi_2\sigma_2-\sigma_{bf}(\phi_1+\phi_2))}{(\phi_1\sigma_1+\phi_2\sigma_2+2\phi\sigma_{bf})-\phi\sigma_{bf}((\phi_1\sigma_1+\phi_2\sigma_2)-\sigma_{bf}(\phi_1+\phi_2))}, \tag{10}$$

where the subscript 1 and 2 shows the physical properties of $Al_2O_3$ and $Cu$ respectively. Total volume concentration of $Al_2O_3$ and $Cu$ is denoted by $\phi$ and given as:

$$\phi=\phi_1+\phi_2. \tag{11}$$

Now let us consider the time-dependent thermal conductivity of the hybrid nanofluid is defined as the form:

$$k_{hnf}(T)=k_{hnf}\left(1+\epsilon\frac{T-T_\infty}{T_w-T_\infty}\right). \tag{12}$$

Following similarity variables are suggested to transfer the Eqs. (2)–(5) into simplified set of differential equations:

$$u=axF'(\eta), v=ayG'(\eta), w=-\sqrt{a\nu_{bf}}(F(\eta)+G(\eta)), \frac{T}{T_\infty}=(\theta_w-1)\theta(\eta)+1, \eta=z\sqrt{\frac{a}{\nu_{bf}}}. \tag{13}$$

By means of the above similarity variables, system of nonlinear partial differential Eqs. (2)–(4) takes the following form:

$$\frac{\nu_{hnf}}{\nu_{bf}}F'''+F''(F+G)-F'^2+2\lambda G'+\frac{\rho_{bf}}{\rho_{hnf}}\frac{(\rho\beta)_{hnf}}{(\rho\beta)_{bf}}Gr\theta=\left(\frac{\rho_{bf}}{\rho_{hnf}}\frac{\sigma_{hnf}}{\sigma_{bf}}Ha+\frac{\nu_{hnf}}{\nu_{bf}}K_p\right)F', \tag{14}$$

$$\frac{\nu_{hnf}}{\nu_{bf}}G'''+G''(F+G)-G'^2-2\lambda F'+\frac{\rho_{bf}}{\rho_{hnf}}\frac{(\rho\beta)_{hnf}}{(\rho\beta)_{bf}}Gr\theta=\left(\frac{\rho_{bf}}{\rho_{hnf}}\frac{\sigma_{hnf}}{\sigma_{bf}}Ha+\frac{\nu_{bnf}}{\nu_{bf}}K_p\right)G', \tag{15}$$

$$\left(\left(\frac{k_{hnf}}{k_{bf}}+Rd(1+(\theta_w-1)\theta)^3\right)\theta'+\frac{k_{hnf}}{k_{bf}}\epsilon\theta\theta'\right)'+\frac{(\rho c_p)_{hnf}}{(\rho c_p)_{bf}}Pr(F+G)\theta'+\frac{\mu_{hnf}}{\mu_{bf}}PrEc(F'+G')^2=0, \tag{16}$$

and the boundary conditions converted as:

$$\begin{cases} F'(0)=1+\delta F''(0), G'(0)=\gamma+\delta G''(0), F(0)+G(0)=S, \theta'(0) \\ =-Bi[1-\theta(0)], \\ F'(\eta\to\infty)=0, G'(\eta\to\infty)=0, \theta(\eta\to\infty)=0. \end{cases} \tag{17}$$

In above system the parameters $Ha$, $K_p$, $\lambda$, $Gr$, $Pr$, $Ec$, $Rd$, $\gamma$, $\delta$, $S$, $Bi$ and $\theta_w$ represents the Hartmann, porosity, rotating, Grashof, Prandtl, Eckert, radiation, stretching ratio, slip, suction ($S>0$)/injection ($S<0$), convective and temperature ratio parameters respectively which defined as:

$$Ha=\frac{B_0^2\sigma_{bf}}{a\rho_{bf}},\ K_p=\frac{\nu_{bf}}{aK_p^*},\ \lambda=\frac{\Omega_0 y}{ax},\ Gr_T=\frac{g\beta_{bf}(\theta_w-1)T_\infty x^3}{\nu^2},$$
$$Re=\frac{ax^2}{\nu},\ Gr=\frac{Gr_T}{Re^2},$$
$$Pr=\frac{\nu_{bf}(\rho c_p)_{bf}}{k_{bf}},\ Ec=\frac{a\mu_{bf}}{(\theta_w-1)T_\infty(\rho c_p)_{bf}},\ Rd=\frac{16\sigma^*T_\infty^3}{3k^*k_{bf}},\ \gamma=\frac{b}{a},$$
$$\delta=\frac{2-\Omega}{\Omega}\Lambda\sqrt{\frac{a}{\nu_{bf}}},\ S=\frac{W}{\sqrt{a\nu_{bf}}},$$
$$Bi=\frac{h_{bf}}{k_{bf}}\sqrt{\frac{\nu_{bf}}{a}},\ \theta_w=\frac{T_w}{T_\infty}. \tag{18}$$

Wall shear stresses $\tau_{wx}$ and $\tau_{wy}$ in $x$ and $y$-direction also local Nusselt number of the stretching surface are respectively given as:

$$\tau_{wx}=\mu_{hnf}\left(\frac{\partial u}{\partial z}\right)_{z=0},\tau_{wy}=\mu_{hnf}\left(\frac{\partial v}{\partial z}\right)_{z=0},$$
$$Nu_x=-\frac{xk_{hnf}}{k_{bf}(\theta_w-1)T_\infty}\left(\frac{\partial T}{\partial z}\right)_{z=0}-\frac{x}{k_{bf}(\theta_w-1)T_\infty}\frac{16\sigma^*}{3k^*}T^3\left(\frac{\partial T}{\partial z}\right)_{z=0}. \tag{19}$$

Non-dimensional form of skin friction and local Nusselt number are given as:

$$\begin{cases} Re_x^{1/2}C_{fx}=\frac{\rho_{bf}}{\rho_{hnf}}\frac{\mu_{hnf}}{\mu_{bf}}F''(0), Re_y^{1/2}C_{fy}=\gamma^{-3/2}\frac{\rho_{bf}}{\rho_{hnf}}\frac{\mu_{hnf}}{\mu_{bf}}G''(0), \\ Re_x^{-1/2}Nu_x=-\left(\frac{k_{hnf}}{k_{bf}}+Rd((\theta_w-1)\theta(0)+1)^3\right)\theta'(0). \end{cases} \tag{20}$$

Here $Re_x^{1/2}=x\sqrt{\frac{a}{\nu_f}}$ and $Re_y^{1/2}=y\sqrt{\frac{a}{\nu_f}}$ are represents the local Reynolds number.

## 3. Least square method and solution procedure

This section is devoted to investigate the numerical solution of the problem (14)-(16) by means of least square approach [7,37,38]. Least square method is simple to apply and easy to understand. The key steps of mentioned scheme are stated under:

**Step 1.** In this method firstly consider the problem given in the Eqs. (14)–(16) and a trial solution is assumed which must satisfy the conditions of the problem given in (17).

**Step 2.** The trial solutions for $F(\eta), G(\eta)$ and $\theta(\eta)$ for solving Eqs. (14)–(16) as given below:

$$\tilde{F}(\eta)=\ddot{\varpi}_0+\ddot{\varpi}_1\eta+\ddot{\varpi}_2\eta^2+\ldots+\ddot{\varpi}_M\eta^M=\sum_{k=0}^{M}\ddot{\varpi}_k\eta^k, \tag{21}$$

$$\tilde{G}(\eta)=\ddot{\varpi}_0+\ddot{\varpi}_1\eta+\ddot{\varpi}_2\eta^2+\ldots+\ddot{\varpi}_M\eta^M=\sum_{k=0}^{M}\ddot{\varpi}_k\eta^k, \tag{22}$$

$$\tilde{\theta}(\eta)=\ddot{\varpi}_0+\ddot{\varpi}_1\eta+\ddot{\varpi}_2\eta^2+\ldots+\ddot{\varpi}_M\eta^M=\sum_{k=0}^{M}\ddot{\varpi}_k\eta^k. \tag{23}$$

Here the order of approximation of least square denoted by $M$. Since the least square method must fulfill the boundary conditions (17). The trial solutions (21)-(23) reduced to the following form after incorporating the boundary conditions (17):

$$\tilde{F}(\eta)=\frac{S}{2}+\left(1-\frac{(S+2\eta_\infty)\delta}{(\eta_\infty+2\delta)\eta_\infty}\right)\eta-\frac{1}{2}\frac{S+2\eta_\infty}{(\eta_\infty+2\delta)\eta_\infty}\eta^2+\sum_{n=1}^{M-3}\ddot{\varpi}_n\left[\eta^{n+1}-\frac{\eta_\infty^{n+1}}{\eta_\infty+2\delta}\eta+\frac{2\delta\eta_\infty^{n+1}}{\eta_\infty+2\delta}\right]\eta, \tag{24}$$

$$\tilde{G}(\eta)=\frac{S}{2}+\left(\gamma-\frac{(S+2\gamma\eta_\infty)\delta}{(\eta_\infty+2\delta)\eta_\infty}\right)\eta-\frac{1}{2}\frac{S+2\gamma\eta_\infty}{(\eta_\infty+2\delta)\eta_\infty}\eta^2+\sum_{n=1}^{M-3}\ddot{\varpi}_n\left[\eta^{n+1}-\frac{\eta_\infty^{n+1}}{\eta_\infty+2\delta}\eta+\frac{2\delta\eta_\infty^{n+1}}{\eta_\infty+2\delta}\right]\eta, \tag{25}$$

$$\tilde{\theta}(\eta)=\frac{\eta_\infty Bi}{1+\eta_\infty Bi}-\frac{Bi}{1+\eta_\infty Bi}\eta+\sum_{n=1}^{M-2}\ddot{\varpi}_n\left[\eta^{n+1}-\frac{\eta_\infty^{i+1}Bi}{1+\eta_\infty Bi}\eta-\frac{\eta_\infty^{i+1}}{1+\eta_\infty Bi}\right]. \tag{26}$$

where assume $\eta_\infty=\infty$.

**Step 3.** We get the following residual $\mathbf{R}_F,\mathbf{R}_G$ and $\mathbf{R}_\theta$ vectors by incorporating the trial solutions into Eqs. (14–16):

$$\mathbf{R}_F=\frac{\nu_{hnf}}{\nu_{bf}}\tilde{F}'''+\tilde{F}''(\tilde{F}+\tilde{G})-\tilde{F}'^2+2\lambda\tilde{G}'+\frac{\rho_{bf}}{\rho_{hnf}}\frac{(\rho\beta)_{hnf}}{(\rho\beta)_{bf}}Gr\tilde{\theta}=\left(\frac{\rho_{bf}}{\rho_{hnf}}\frac{\sigma_{hnf}}{\sigma_{bf}}Ha+\frac{\nu_{hnf}}{\nu_{bf}}K_p\right)\tilde{F}', \tag{27}$$

$$\mathbf{R}_G=\frac{\nu_{hnf}}{\nu_{bf}}\tilde{G}'''+\tilde{G}''(\tilde{F}+\tilde{G})-\tilde{G}'^2-2\lambda\tilde{F}'+\frac{\rho_{bf}}{\rho_{hnf}}\frac{(\rho\beta)_{hnf}}{(\rho\beta)_{bf}}Gr\tilde{\theta}=\left(\frac{\rho_{bf}}{\rho_{hnf}}\frac{\sigma_{hnf}}{\sigma_{bf}}Ha+\frac{\nu_{bnf}}{\nu_{bf}}K_p\right)\tilde{G}', \tag{28}$$

$$\mathbf{R}_\theta=\left(\left(\frac{k_{hnf}}{k_{bf}}+Rd(1+(\theta_w-1)\tilde{\theta})^3\right)\tilde{\theta}'+\frac{k_{hnf}}{k_{bf}}\epsilon\tilde{\theta}\tilde{\theta}'\right)'+\frac{(\rho c_p)_{hnf}}{(\rho c_p)_{bf}}Pr(\tilde{F}+\tilde{G})\tilde{\theta}'+\frac{\mu_{hnf}}{\mu_{bf}}PrEc(\tilde{F}'+\tilde{G}')^2\neq 0. \tag{29}$$

**Step 4.** By means of the above residual, we get the following functions:

$$\mathbf{E}_F=\int_\Gamma\mathbf{R}_F^2\mathrm{d}\eta,\mathbf{E}_G=\int_\Gamma\mathbf{R}_G^2\mathrm{d}\eta,\mathbf{E}_\theta=\int_\Gamma\mathbf{R}_\theta^2\mathrm{d}\eta. \tag{30}$$

Here $\Gamma=[0,\infty]$. In order to minimize the functions above functions the derivatives of the functions w.r.t $\varpi_i$'s essential be zero.

$$\frac{\partial\mathbf{E}_F}{\partial\ddot{\varpi}_i}=2\int\mathbf{R}_F(\eta)\frac{\partial\mathbf{R}_F}{\partial\ddot{\varpi}_i}\mathrm{d}\eta=0,\quad i=0,1,2,\ldots,M, \tag{31}$$

$$\frac{\partial\mathbf{E}_G}{\partial\ddot{\varpi}_i}=2\int\mathbf{R}_G(\eta)\frac{\partial\mathbf{R}_G}{\partial\ddot{\varpi}_i}\mathrm{d}\eta=0,\quad i=0,1,2,\ldots,M, \tag{32}$$

$$\frac{\partial\mathbf{E}_\theta}{\partial\ddot{\varpi}_i}=2\int\mathbf{R}_\theta(\eta)\frac{\partial\mathbf{R}_\theta}{\partial\ddot{\varpi}_i}\mathrm{d}\eta=0,\quad i=0,1,2,\ldots,M. \tag{33}$$

Nonetheless, the "2" coefficient can be dropped.

**Step 5.** We get the values of all unknowns $\varpi$'s after solving the system of algebraic equations achieved in last step. Consequently, the approximate solution obtained after incorporating the values of all $\varpi$'s.

## 4. Results and discussion

In this section, results are demonstrated the physical aspects of the present model, which is formulated in the previous section. For this purpose, graphical behavior of flow and heat transfer at the surface of sheet are determined in form of skin friction and Nusselt number with respect to the involved parameters namely: Hartmann, porosity, rotating, Grashof, Prandtl, Eckert, radiation, stretching ratio, slip, suction/injection and convective parameters.

In order to observe the behavior of the friction and rate of heat transfer at boundaries, the skin friction coefficient and Nusselt number are plotted (see Figs. 1–3) for different values of parameters. In Figs. 1 and 2, behavior of skin friction coefficient for different values of the parameters is explained. It is clear from Fig. 1(a) that velocity is decreasing at the surface because of increasing

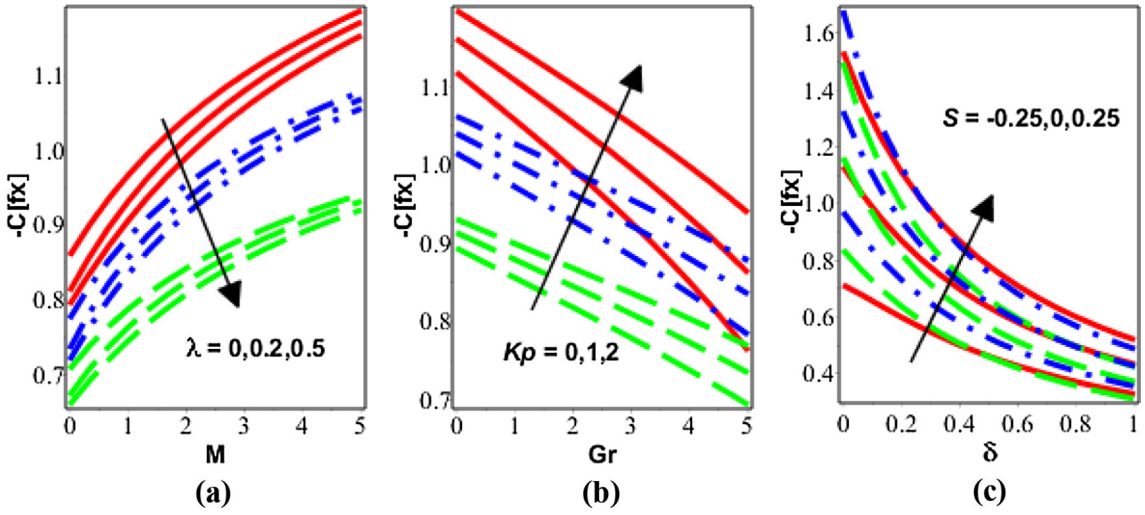


**Fig. 1.** Variation in $C_{fx}$ as varying (a) $\lambda$ and $M$, (b) $Gr$ and $Kp$, (c) $S$ and $\delta$.

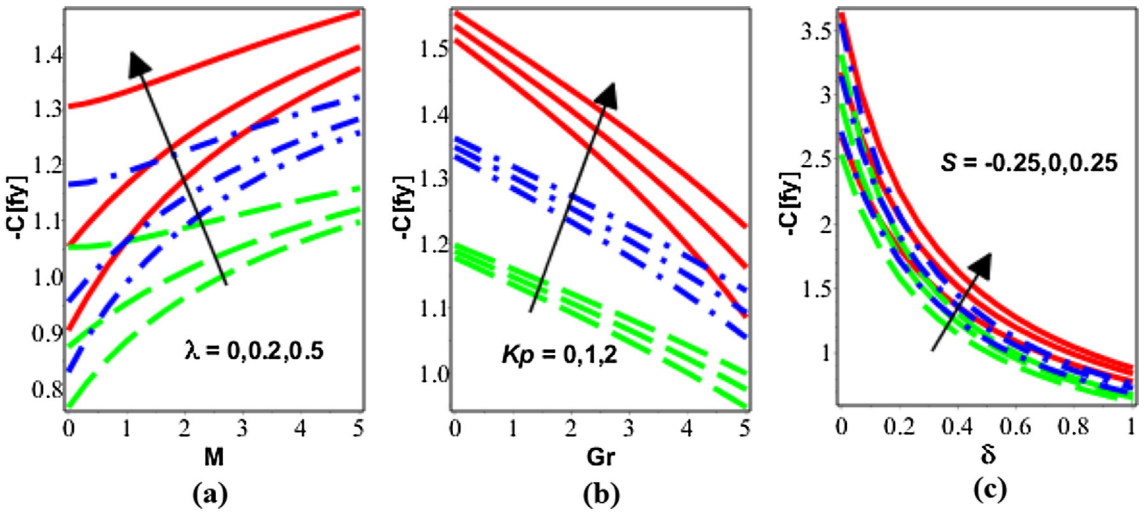


**Fig. 2.** Variation in $C_{fy}$ as varying (a) $\lambda$ and $M$, (b) $Gr$ and $Kp$, (c) $S$ and $\delta$.

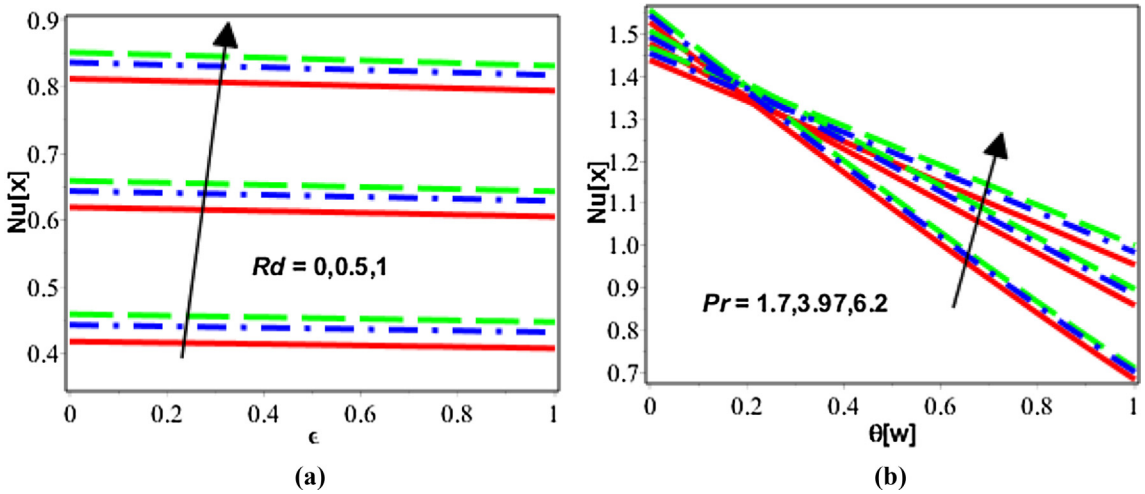


**Fig. 3.** Variation in $Nu_x$ as varying (a) $Rd$ and $\epsilon$, (b) $Pr$ and $\theta_w$.

values of rotation effects. This is because of rotational forces which produce resistance to flow the fluid in $x$ direction. These forces produce the resistance in $x$ direction but enhance the velocity in $y$ dirction. Therefore, reverse behavior of the velocity can be seen in Fig. 2(a). By increasing the values of $K_P$, it is observed that skin friction along ($x$ and $y$ directions) is intense gradually. The physical reason behind this happening is permeability of the medium that support fluid flow. In the next, Figs. 1(c) and 2(c) are plotted to explain the behavior of velocity for suction and injection cases. Both the cases have increasing behavior due to the increasing values of $S$.

In case of temperature, Nusselt number is plotted for various values $Pr$ and $Rd$. An increase in the values of both parameters, temperature shows opposite behavior i.e., temperature is increasing at boundaries for increasing values of $Rd$ and increasing for increasing values of Prandtl number. Basically, due to the radiation effects temperature of the fluid is increasing (see 9(b)) at the center of the geometry therefore Fig. 3(a) is plotted to validate this phenomenon.

In Figs. 4–9, behavior of velocity for different values of parameters are plotted. In Fig. 4(a) behavior of velocity for variated values of Hartman number is explained. It is clear from this Fig. 4(a) that velocity is decreasing with an increase in Hartman number. As we know that Hartmann number appears in the expressed model is due to the implementation of magnetic field and this factor of the system oppose the flow of fluid. Therefore, velocity is decreasing. Oppositely, an increasing behavior of $y-$ component of velocity profile is observed in Fig. 4(b). This is due to the rotation effects which supports the $y-$ component of velocity.

In the Fig. 5(a and b), velocity profile is decreasing for both $x$ and $y-$ component velocity because increasing values of rotation parameter produce resistive forces against velocity. Hence velocity is decreasing. In Fig. 6(a and b), behavior of velocity for variated values of $Gr$ is characterized. It is clear from the represented Fig. 6(a) and (b) that Grashof number is supported to enhance the velocity of the nanofluid. In the next Fig. 7(a) and (b), graphical behavior of velocity for growing values of porosity parameter is signified. Velocity of the system is decreasing because of two factors. One of the factor is the directly relationship between porosity parameter and viscosity. With the increase of this parameter viscosity of the fluid increase and hence velocity decrease. Secondly, when porosity of the system is increasing gradually then velocity profile is disturbed which become the cause of reduction of velocity. Fig. 8 is plotted to cover the area of slip parameter and observation regarding these figures show that velocity is decaling. When slip parameter increase, the area to flow the fluid increase and

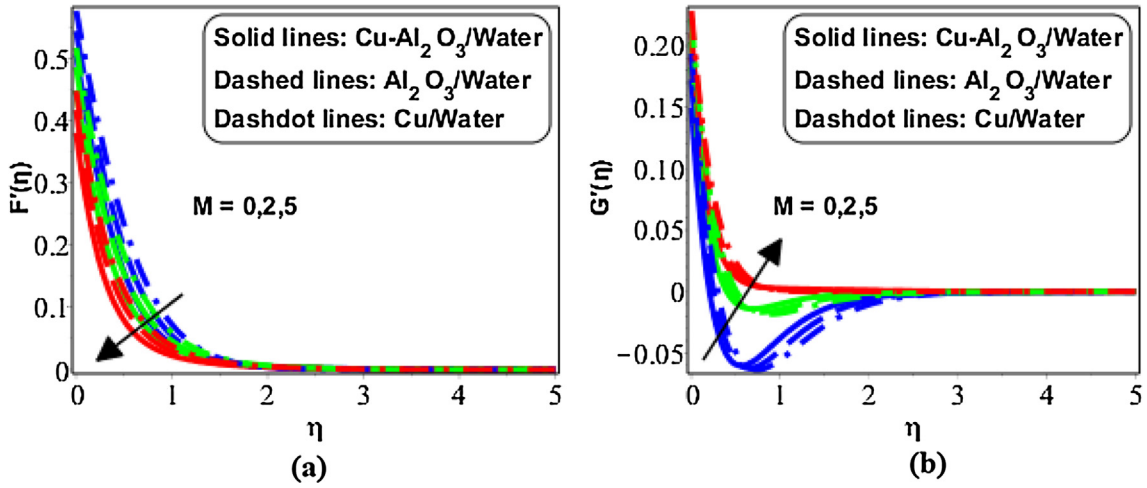


**Fig. 4.** Variation in (a) $F'(\eta)$ and (b) $G'(\eta)$ for various values of $M$ when $\delta = K_p = 0.5$, $Gr = 2$, $\gamma = 0.7$, $S = 0.8$, $\lambda = 1.5$.

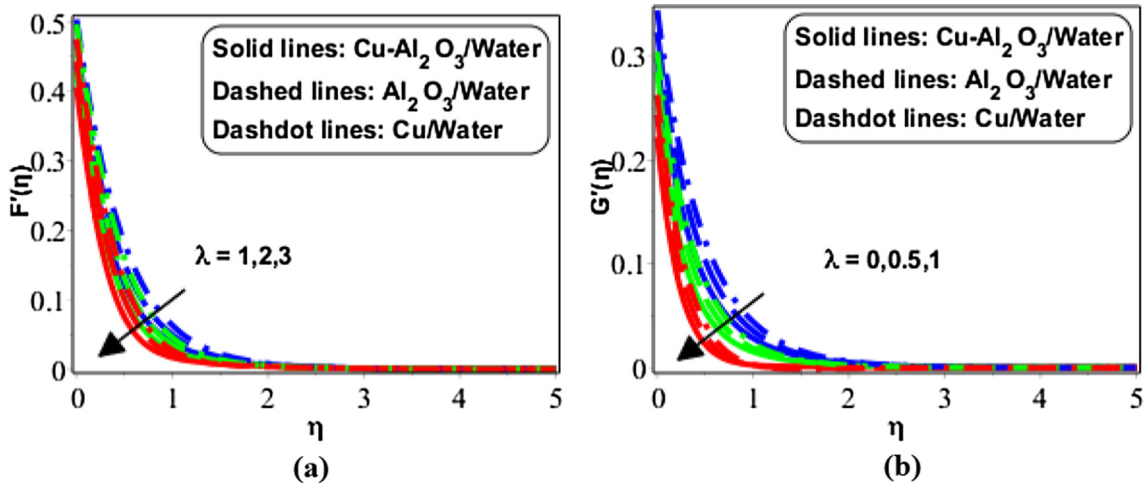


**Fig. 5.** Variation in (a) $F'(\eta)$ and (b) $G'(\eta)$ for various values of $\lambda$ when $\delta = K_p = 0.5$, $M = 2.5$, $Gr = 2$, $\gamma = 0.7$, $S = 0.8$, $M = 2.5$.

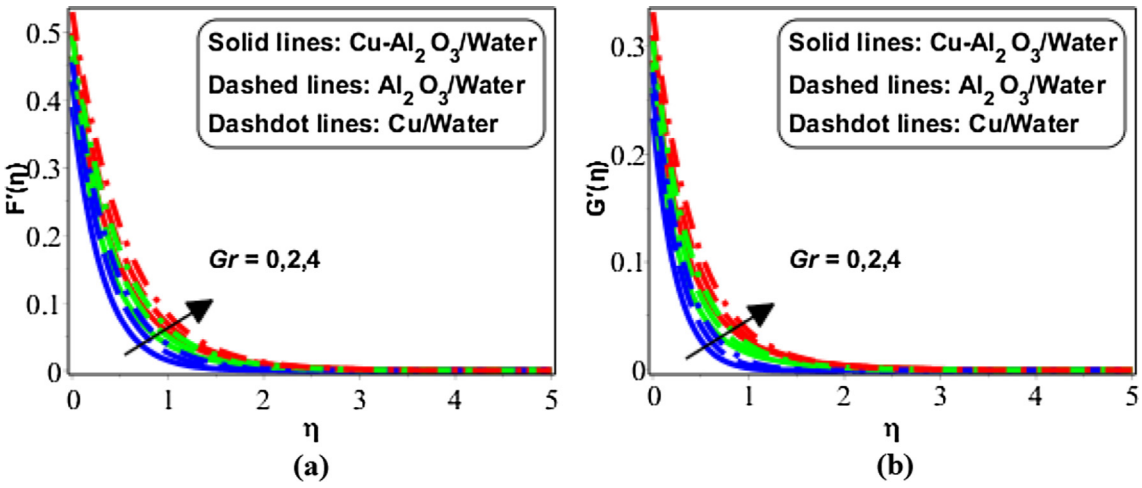


**Fig. 6.** Variation in (a) $F'(\eta)$ and (b) $G'(\eta)$ for various values of $Gr$ when $\delta = K_p = 0.5,\ M = 2.5,\ \gamma = 0.7,\ S = 0.8,\ \lambda = 0.5,\ M = 2.5$.

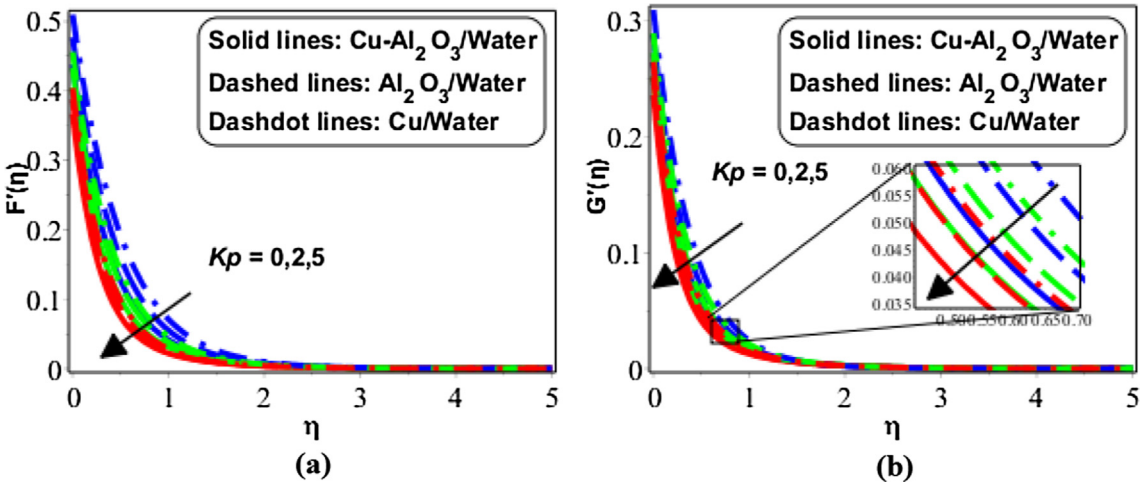


**Fig. 7.** Variation in (a) $F'(\eta)$ and (b) $G'(\eta)$ for various values of $Kp$ when $\delta = 0.5, M = 2.5, \gamma = 0.7, S = 0.8, \lambda = 0.5, M = 2.5, Gr = 2$.

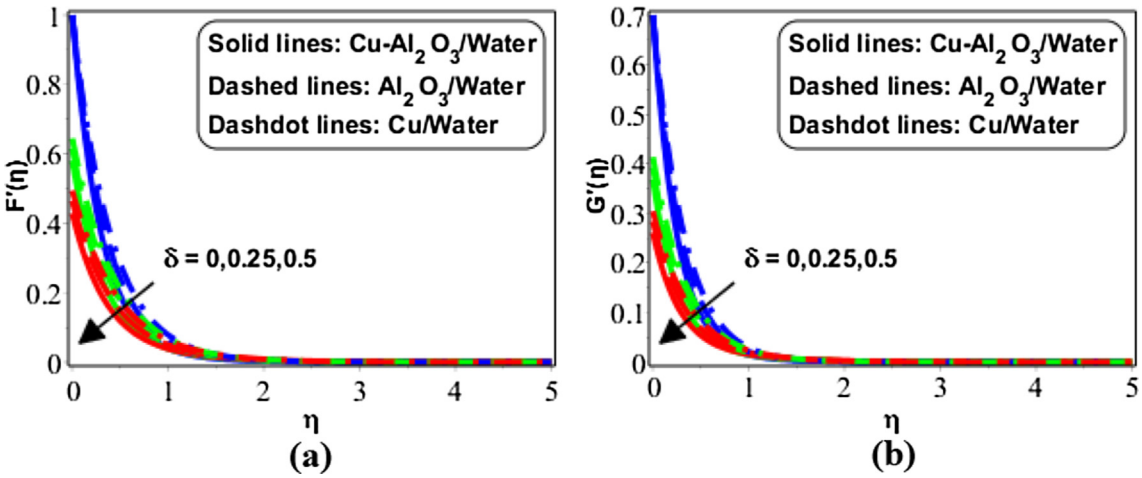


**Fig. 8.** Variation in (a) $F'(\eta)$ and (b) $G'(\eta)$ for various values of $\delta$ when $K_p = 0.5,\ M = 2.5,\ \gamma = 0.7,\ S = 0.8,\ \lambda = 0.5,\ M = 2.5,\ Gr = 2$.

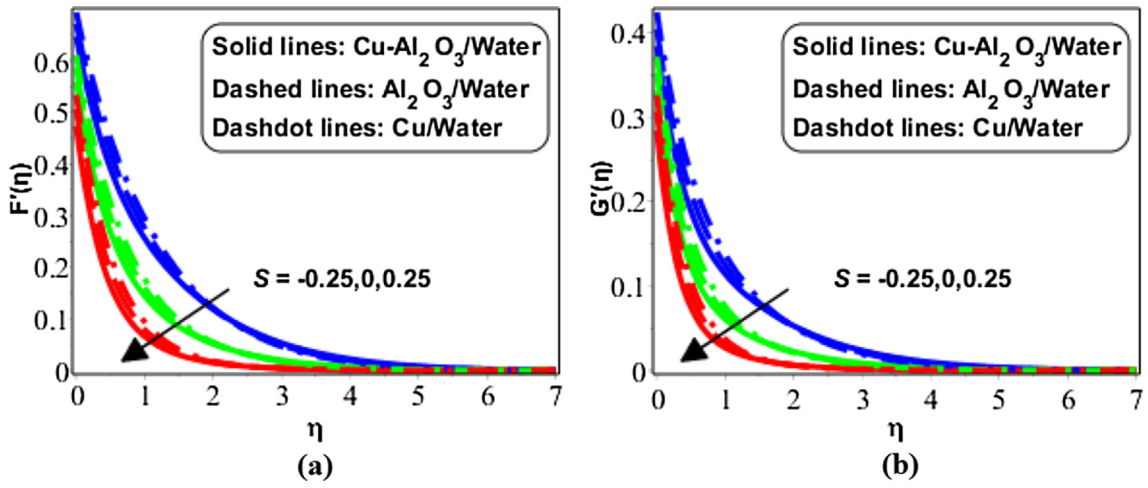


**Fig. 9.** Variation in (a) $F'(\eta)$ and (b) $G'(\eta)$ for various values of $S$ when $\delta = K_p = 0.5$, $M = 2.5$, $\gamma = 0.7$, $\lambda = 0.5$, $M = 2.5$, $Gr = 2$.

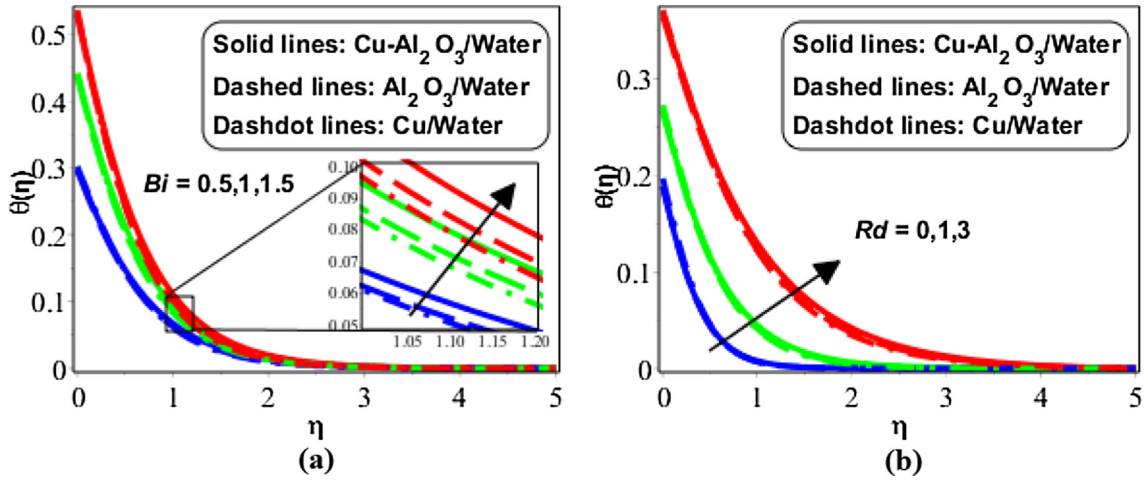


**Fig. 10.** Variation in $\theta(\eta)$ as varying (a) $Bi$ for $Rd = 1.5$ (b) $Rd$ for $Bi = 0.5$ when $\delta = K_p = 0.5$, $M = 2.5$, $\gamma = 0.7$, $S = 0.8$, $\lambda = 0.5$, $M = 2.5$, $Gr = 2$, $Pr = 3.97$, $Ec = 0.5$, $\epsilon = 0.7$, $\theta_w = 0.8$.

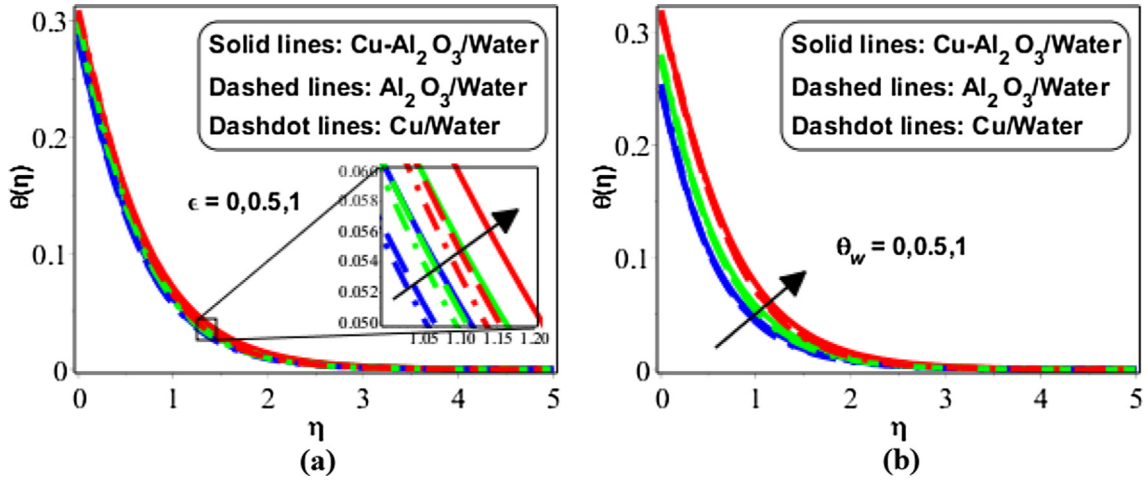


**Fig. 11.** Variation in $\theta(\eta)$ as varying (a) $\epsilon$ for $\theta_w = 0.8$ (b) $\theta_w$ for $\epsilon = 0.7$ when $\delta = K_p = 0.5, M = 2.5, \gamma = 0.7, S = 0.8, \lambda = 0.5, M = 2.5, Gr = 2, Pr = 3.97$, $Ec = 0.5, Rd = 1.5, \theta_w = 0.8, Bi = 0.5$.

**Table 1**
Thermophysical properties of base fluids and nanoparticles [41].

| Properties | $k$(W/mK) | $\rho$(kg/m$^3$) | $c_p$(Jk/gK) | $\sigma$(μS/cm) | $\beta \times 10^5$(K$^{-1}$) |
|---|---|---|---|---|---|
| Water | 0.613 | 997.1 | 4179 | 0.05 | 21 |
| $Cu$ | 400 | 8933 | 385 | $5.96\times10^7$ | 1.67 |
| $Al_2O_3$ | 40 | 3940 | 765 | $1\times10^{-10}$ | 0.85 |

**Table 2**
Comparison of the numerical values of skin friction coefficients achieved by Galerkin method with published results [33] for numerous values of $\alpha$ and $M$.

| $M$ | $\alpha$ | $-Re_x^{1/2}C_{fx}$ | | $-Re_y^{1/2}C_{fy}$ | |
|---|---|---|---|---|---|
| | | [40] | LSM | [40] | LSM |
| 0.0 | 0.2 | 1.1815 | 1.181536 | 2.6420 | 2.641994 |
| 0.3 | | 1.2192 | 1.219150 | 2.7261 | 2.726104 |
| 0.5 | | 1.2833 | 1.282642 | 2.8695 | 2.869466 |
| 0.1 | 0.1 | 1.1357 | 1.135663 | 3.5913 | 3.591282 |
| | 0.3 | 1.2339 | 1.233854 | 2.2527 | 2.252698 |
| | 0.5 | 1.3248 | 1.324787 | 1.8735 | 1.873532 |

finally velocity of the system decrease. In the next Fig. 9 suction ($S > 0$)/injection ($S < 0$) parameter effects on velocity is sketched. Velocity of the system is decreasing in this case because due to suction and injection process, fluid is entering and leaving from the porous.

Further Figs. 10 and 11, are plotted to explain the attitude of temperature for different and increasing values defined parameters. Fig. 10 is explaining the reaction of temperature profile for rising values of convective parameter. Basically, this parameter appears at the boundary of the system and is very helpful to enhance the temperature. This temperature is shift further from the boundaries to internal system. As a result, temperature of the whole system is increasing with the increase of this parameter (see Fig. 10(a)). Further temperature of the formulated system is raising with the increasing values of radiation parameter (see Fig. 10(b)). It is very easy to understand that applied radiations is providing energy to the particles of the nanofluid. Therefore temperature of the system is enhancing. In Fig. 11(a and b), temperature profile is raising due the increasing effects of $\epsilon$ and $\theta_w$. It is important to nominate here that $\epsilon = 0$ is the case, when thermal conductivity of the system is constant.

All the plotted Fig. 11 in above picture are divided into three categories. Dash-dot, dashed and solid lines are explaining the behavior of velocity and temperature for $Cu$-water (regular), $Al_2O_3$-water (regular) and $Cu$-$Al_2O_3$-water (hybrid) nanofluid respectively. Observation shows that hybrid nanofluid has high velocity and temperature. Therefore, we can say that hybrid technology may helpful to enhance the physical properties of the fluid. For this sense, we can minimize the cost effects.

Table 1 shows the Thermophysical properties of pure water and nanoparticles. Table 2 construct to execute the efficiency of proposed least square method. From this table it is confirm that the proposed method is excellent agreement with published work [40] and well-matched to investigate the solutions of the proposed problem.

## 5. Conclusion

In the current study, three-dimensional rotating flow of $Cu$-$Al_2O_3$-water hybrid nanofluid over a permeable linear stretching sheet under the impact of nonlinear thermal radiation and time-dependent thermal conductivity is analyzed. Simplified set of ODEs obtained with the help of suggested similarity variables. The approximate solution of simplified ODEs in attained with the help of least square technique. Hence, key findings are enlisted below:

- Velocity profiles $F'(\eta)$ and $G'(\eta)$ for the case of $Cu$-$Al_2O_3$-water is dominant as compare to $Cu$-water and $Al_2O_3$-water.
- Temperature of the fluid is low for the case of $Cu$-$Al_2O_3$-water as compare to $Cu$-water and $Al_2O_3$-water.
- Solution obtained via least square method is excellent in agreement with RK-4 and published results, which shows the efficiency and reliability of the proposed method.
- Nusselt number increases due to the variation of Prandtl number and decreases against the variation in temperature ratio, thermal radiation and nonlinear thermal radiation.
- By variating the Hartmann number, porosity parameter and suction/injection parameters, skin friction coefficient increases and reverse behavior is achieved by increasing the values of rotational parameter, Grashof number and slip parameter.

## Conflict of interest

There is no actual or potential conflict of interest including any financial, personal or other relationships with other people or organizations.

## References

[1] D. Singh, J. Tourbort, G. Chen, Heavy vehicle Systems Optimization Merit Review and Peer Evaluation, Annual Report, Argonne National Laboratory, 2006.
[2] M. Usman, M. Hamid, U. Khan, S.T. Mohyud-Din, M.A. Iqbal, W. Wang, Differential transform method for unsteady nanofluid flow and heat transfer, Alexandria Eng. J. (2017), https://doi.org/10.1016/j.aej.2017.03.052.
[3] M. Sheikholeslami, M.K. Sadoughi, Simulation of CuO-water nanofluid heat transfer enhancement in presence of melting surface, Int. J. Heat Mass Transf. 116 (2018) 909–919.
[4] M. Usman, M. Hamid, S.T. Mohyud-Din, A. Waheed, W. Wang, Exploration of uniform heat flux on the flow and heat transportation of ferrofluids along a smooth plate: comparative investigation, Int. J. Biomath. 11 (2) (2018) 1850048.
[5] M. Sheikholeslami, S.A. Shehzad, Numerical analysis of $Fe_3O_4$–$H_2O$ nanofluid flow in permeable media under the effect of external magnetic source, Int. J. Heat Mass Transf. 118 (2018) 182–192.
[6] M. Hamid, M. Usman, T. Zubair, R.U. Haq, W. Wang, Shape effects of $MoS_2$ nanoparticles on rotating flow of nanofluid along a stretching surface with variable thermal conductivity: a Galerkin approach, Int. J. Heat Mass Transf. 124 (2018) 706–714.
[7] J. Li, H. Zhou, Y. Zhang, S.A. Shahzad, M. Yang, Z. Hu, C. Yu, Tuning of the perylene probe excimer emission with silver nanoparticles, Anal. Chim. Acta 1016 (2018) 40–48.
[8] M. Usman, M. Hamid, R.U. Haq, W. Wang, Heat and fluid flow of water and ethylene-glycol based Cu-nanoparticles between two parallel squeezing porous disks: LSGM approach, Int. J. Heat Mass Transf. 123 (2018) 888–895.
[9] Z. Han, B. Yang, S. Kim, M. Zachariah, Application of hybrid sphere/carbon nanotube particles in nanofluids, Nanotechnology 18 (2007) 105701.

[10] S. Jan, A. Khojin, W. Zhong, Enhancement of fluid thermal conductivity by addition of single and hybrid nano-additives, Thermochim. Acta 462 (2007) 45–55.
[11] G. Paul, J. Philip, B. Raj, P. Das, I. Manna, Synthesis, characterization and thermal property measurement of nano-Al96Zn05 dispersed nanofluid prepared by a two-step process, Int. J. Heat Mass Transf. 54 (2011) 8–3783.
[12] J. Sarkar, P. Ghosh, A. Adil, A review on hybrid nanofluids: resent research, development and applications, Renew. Sustain. Energy Rev. 43 (2015) 164–177.
[13] C. Ho, J. Huang, P. Tsai, Y. Yang, Prepration and properties of hybrid water based suspension of $Al_2O_3$ nanoparticles and MEPCM particles a functional forced convection fluid, Int. Commum. Heat Mass Transf. 37 (2010) 490–494.
[14] S. Botha, P. Ndungu, B. Bladergroen, Physicochemical properties of oil based nanofluids containing hybrid structures of silver nanoparticle supported on silica, Ind. Eng. Chem. Res. 50 (2011) 3071–3077.
[15] A. Chamkha, I. Miroshnichenko, M. Sheremet, Numerical analysis of unsteady conjugate natural convection of hybrid water-based nanofluid in a semicircular cavity, J. Therm. Sci. Eng. Appl. 9 (2017) 041004.
[16] L. Crane, Flow past a stretching plate, Zeitschrift für Angewandte Mathematik und Physik 21 (1970) 645–647.
[17] C. Wang, Stretching a surface in a rotating fluid, Zeitschrift für Angewandte Mathematik und Physic 39 (2) (1988) 177–185.
[18] H. Takhar, G. Nath, Unsteady flow over a stretching surface with a magnetic field in a rotating fluid, Zeitschrift für Angewandte Mathematik und Physic 49 (6) (1998) 989–1001.
[19] H. Andersson, Slip flow past a stretching surface, Acta Mech. 158 (2002) 121–125.
[20] R. Nazar, N. Amin, I. Pop, Unsteady boundary layer flow due to a stretching surface in a rotating fluid, Mech. Res. Comm.s 31 (2004) 8–121.
[21] E. Eldahab, M. Aziz, Blowing/suction effect on hydromagnetic heat transfer by mixed convection from an inclined continuously stretching surface with internal heat generation/absorption, Int. J. Ther. Sci. 43 (2004) 19–709.
[22] M. Kumari, T. Grosan, I. Pop, Rotating flow of power-law fluids over a stretching surface, J. Taiwan Insti. Chem. Eng. 26 (2006) 11–19.
[23] K. Govardhan, B. Balaswamy, N. Kishan, Unsteady boundary layer flow due to a stretching porous surface in a rotating fluid, Eng. Mech. 21 (2014) 269–277.
[24] Masood Khan Hashim, A revised model to analyze the heat and mass transfer mechanisms in the flow of Carreau nanofluids, Int. J. Heat Mass Transf. 103 (2016) 291–297.
[25] Hashim, M. Khan, Critical values in flow patterns of Magneto-Carreau fluid over a circular cylinder with diffusion species: multiple solutions, J. Taiwan Inst. Chem. Eng. 77 (2017) 282–292.
[26] M. Khan, Hashim, Abdul Hafeez, A review on slip-flow and heat transfer performance of nanofluids from a permeable shrinking surface with thermal radiation: dual solutions, Chem. Eng. Sci. 173 (2017) 1–11.
[27] Hashim, M. Khan, Ali Saleh Alshomrani, Numerical simulation for flow and heat transfer to Carreau fluid with magnetic field effect: dual nature study, J. Magn. Magn. Mater. 443 (2017) 13–21.
[28] Hashim, M. Khan, Ali Saleh Alshomrani, Characteristics of meltingheat transfer during flow of Carreau fluid induced by a stretching cylinder, Euro. Phys. J. E 40 (2017) 8.
[29] S. Shateyi, G. Tendayi, Numerical analysis of unsteady MHD flow near a stagnation point of a two-dimensional porous body with heat and mass transfer, Therm. Radiat. Chem. React. Bou. Val. Prob. 5 (2014) 218.
[30] T. Hayat, T. Muhammad, A. Qayyum, A. Alseadi, M. Mustafa, On squeezing flow of nanofluid in the presence of magnetic field effects, J. Mol. Liquid 213 (2016) 179–185.
[31] Y. Lin, L. Zhang, X. Zhang, L. Ma, G. Chen, MHD pseudo-plastic nanofluid unsteady flow and heat transfer on the finite thin film on a stretching surface internal heat generation, Int. J. Heat Mass Transf. 84 (2015) 903–911.
[32] R. Haq, S. Nadeem, Z.H. Khan, N. Noor, MHD squeezed flow of water functionalized metallic nanoparticles over a sensor surface, Physica E 73 (2015) 45–53.
[33] A. Ishak, Thermal boundary layer flow over a stretching sheet in a micropolar fluid with radiation effect, Meccanica 45 (2010) 367–373.
[34] T. Hayat, M. Qasim, Z. Abbas, Radiation and mass transfer effects on the magnetohydrodynamic unsteady flow induced by a stretching sheet, Z. Naturforsch. 65a (2010) 231–239.
[35] S. Shateyi, J. Prakash, A new numerical approach for MHD laminar boundary layer flow and heat transfer of nanofluids over a moving surface in the presence of thermal radiation, Bou. Val. Prob. (2014) 2.
[36] W. Khan, O. Makinde, Z. Khan, Non-aligned MHD stagnation point flow of variable viscosity nanofluid past a stretching sheet radiative heat, Int J. Heat Mass Transf. 96 (2016) 525–534.
[37] S.T. Mohyud-Din, M. Usman, K. Afaq, M. Hamid, W. Wang, Examination of carbon-water nanofluid flow with thermal radiation under the effect of Marangoni convection, Eng. Comput. 34 (7) (2017) 2330–2343.
[38] M. Usman, R.U. Haq, M. Hamid, W. Wang, Least square study of heat transfer of water based Cu and Ag nanoparticles along a converging/diverging channel, J. Mol. Liquids 249 (2018) 856–867.
[39] T. Hayat, A. Aziz, T. Muhammad, A. Alsaedi, Three-dimensional flow of nanofluid with heat and mass flux boundary conditions, Chin. J. Phys. 55 (4) (2017) 1495–1510.
[40] T. Hayat, M. Khan, T. Muhammad, A. Alsaedi, On model for three dimensional flow of nanofluid with heat and mass flux boundary conditions, J. Therm. Sci. Eng. Appl. (2017), https://doi.org/10.1115/1.4038700.
[41] A.M. Rashad, A.J. Chamkha, M. Ismael, T. Salah, Magnetohydrodynamics natural convection in a triangular cavity filled with a Cu-$Al_2O_3$/water hybrid nanofluid with localized heating from below and internal heat generation, J. Heat Transf. (2018).